https://doi.org/10.5194/egusphere-2026-4511
Preprint. Discussion started: 17 August 2026

Fractal Geometry of Aerosol Particles and Its Impact on Atmospheric Optical Properties: Development and Validation of the Fractal Aerosol Cluster Model in a Heavy Haze Event

Liu Zhenxin[1†], Li Weimin[1], Zhang Bihui[2], Li Xiaolan[3], Mao Yuhao[1], Zhang Kuan[1], Ma Xinye[1], Liao Hong[1†]

[1] Jiangsu Key Laboratory of Intelligent Atmospheric Environment Monitoring and Carbon–Pollution Co-control /Jiangsu Collaborative Innovation Center of Atmospheric Environment and Equipment Technology, School of Environmental Science and Engineering, Nanjing University of Information Science and Technology (NUIST), Nanjing 210044, China.

[2] National Meteorological Centre, China Meteorological Administration, Beijing, 100081, China.

[3] Institute of Atmospheric Environment, China Meteorological Administration, Shenyang 110166, P. R. China/Shenyang Academy of Agricultural and Ecological Meteorology, Chinese Academy of Meteorological Sciences, Shenyang 110166, P. R. China;

Corresponding author: Liu Zhenxin (liuzhenxin@nuist.edu.cn) , Liao Hong (hongliao@nuist.edu.cn)

Key Points:

- A Fractal Aerosol Cluster Model (**FACM**) was developed to better reproduce the growth of the aerosol cluster and quantify its optical and aerodynamic equivalent size.
- The fractal geometry features of the aerosol cluster, assumed to be formulated by random diffusion and aggregation of monomeric particles, leads to the larger optical and less aerodynamic equivalent radius, compared to most of current model in which the aerosol particles assumed to be spherical shapes.
- The FACM was coupled to WRF-Chem and sensitivity experiments of a heavy haze event were conducted. Better performance of atmospheric visibility by FACM-WRF-Chem was confirmed than the control case of WRF-Chem when comparing with the observations.

https://doi.org/10.5194/egusphere-2026-4511
Preprint. Discussion started: 17 August 2026

Abstract

Aerosol particles, as crucial atmospheric components, significantly influence optical properties and play an important role in climate change. Based on Lorenz-Mie's theory, the optical equivalent radius of aerosol particle affects the atmosphere visibility. Traditional aerosol models, which assume spherical or other geometrically regular particle shapes, significantly deviate from observations in visibility simulations. In this study, the mechanism of random diffusion and aggregation of monomeric particles into fractal geometrical clusters was reproduced. The Fractal Aerosol Cluster Model (FACM) was developed to parameterize the optical and aerodynamic sizes of the fractal geometry of aerosol particles. Sensitivity experiments were conducted to simulate a severe haze event in northern China in November 2018 by coupling FACM into WRF-Chem as the experimental case (EXP) while the control case (CTR) by the original WRF-Chem. The simulated near-ground $PM_{2.5}$ concentrations in both EXP and CTR are similar to the observations (OBS). However, EXP simulated the larger extinction coefficients and lower atmospheric visibility (AV), which is more closely to OBS. The average normalized mean error of AV by EXP to OBS is 163.39%, compared to 421.62% by CTR. Thus, considering the fractal geometry of aerosol particles significantly improves simulated AV. Furthermore, a reduction of approximately 60 $W \cdot m^{-2}$ in land surface shortwave radiation in EXP than those by CTR was also confirmed by observations. This study of the optical properties of the fractal aerosol cluster will contribute to future research of atmospheric environment and climate change forcing.

Plain Short Summary

Aerosol particles affect how sunlight travels through the atmosphere, influencing air quality and climate. Traditional models treat these particles as solid spheres, but real-world particles—especially from vehicle exhaust and industrial emissions—often form fluffy, cluster-like structures. This "fluffiness" means they block light far more effectively than solid particles of the same mass. Our study introduces a new model that captures this critical feature. When incorporated into a weather and air quality model and tested during a severe winter haze event in northern China, the new model much more accurately predicted how much light haze would block—a key factor for visibility and surface temperature. Compared to traditional models, it reduced visibility errors by more than half and showed that these fluffy particles reduce sunlight at the surface far more than previously thought, matching real measurements. These findings explain why haze can be so dark and why traditional models often overestimate visibility, improving our ability to forecast air pollution and assess its climate impacts.

1 Introduction

Atmospheric visibility (AV) is not only a key meteorological indicator of air quality but also a critical factor affecting traffic safety and human activities. It is determined by the extinction coefficient, which quantifies the combined scattering and absorption of light by cloud droplets, fog droplets, atmospheric molecules, and aerosol particles. Furthermore, through its influence on solar radiation transfer, AV plays an important role in the surface energy balance and regional climate forcing.

In recent years, severe and rapid degradation of atmospheric visibility happened in and around the urban region caused by worse situation of air quality. The study by Che (2007) indicates that the

https://doi.org/10.5194/egusphere-2026-4511
Preprint. Discussion started: 17 August 2026

AV trends of decreasing in Northern China over the past fifty years were mainly contributed by emissions from human activities (Nah, et al., 2018; Zhou, et al., 2018; Wenfei, et al., 2021; H. Wang, et al., 2024).

Most current atmospheric models, such as WRF-Chem, adopt the Lorenz–Mie theory (Mie, 1908) under the simplifying assumption that aerosol particles are spherical (Fast, Gustafson, et al., 2006). In this framework, the extinction coefficient is determined by the optical equivalent radius of the particles (Wriedt, 2012). This spherical approximation performs reasonably well for pollution events dominated by hygroscopic aerosols, which tend to approach spherical shapes under high humidity due to surface tension effects (Bai, et al., 2018) .

However, during pollution episodes dominated by anthropogenic emissions—particularly from industrial combustion, traffic, and residential heating (Panda&Das, 2017; Xu, et al., 2019)—simulated AV often exhibits large discrepancies from observations, with errors reaching up to 60% (von Hoyningen-Huene&Posse, 1997) . Microscopic observations have revealed that such anthropogenic aerosols possess highly irregular, non-spherical geometries (Veghte&Freedman, 2014; Ishimoto, et al., 2019). Among these, soot and black carbon particles are particularly important: they form through the aggregation of smaller monomeric spherules into chain-like or cluster-like structures (Romshoo, et al., 2021). These structure have some kind of the self-similar, fractal characteristics in the particle size scale range of roughly 0.1 μm - 1 μm (Strawa, et al., 1999). This fractal morphology fundamentally distinguishes them from compact three-dimensional objects (Tiwari, et al., 2016; Wagh, et al., 2023).

Recognizing the importance of particle shape, some models have incorporated non-spherical representations using approaches such as the T-matrix method(Mishchenko, et al., 1996). While suitable for specific regular shapes, these methods face difficulties in accurately representing the complex, random structures of fractal aggregates and incur high computational costs (C. Liu, 2019). More recently, several studies have attempted to refine aerosol optical parameterizations by incorporating fractal geometry (E.&M., 2015; Z. Wang, et al., 2022; G. Chen, et al., 2024; X. Wang, et al., 2025), collectively demonstrating that improved morphological characterization can significantly enhance the accuracy of simulated aerosol optical properties (Y. Wang, et al., 2021).

Despite these advances, a critical gap remains: existing approaches either treat non-spherical particles as three-dimensional objects with compact interiors or lack a direct, analytically tractable link between the fractal growth process and the resulting optical and aerodynamic properties. Moreover, most fractal aerosol schemes have not been online coupled into regional meteorology–chemistry models, limiting their ability to capture the fully interactive aerosol–radiation–meteorology feedbacks that are crucial during heavy haze events.

To address these gaps, this study develops the Fractal Aerosol Cluster Model (FACM). First, we employ a Diffusion-Limited Aggregation (DLA) algorithm to simulate the growth of aerosol clusters from monomeric particles, confirming their fractal geometry via box-counting analysis. Second, we derive explicit analytical relationships between the fractal dimension, the radius of gyration, and the optical and aerodynamic equivalent radii of fractal clusters. These relationships are then parameterized into the FACM. Third, we online couple FACM into the WRF-Chem model (V4.3) and conduct sensitivity experiments for a severe winter haze event over the North China Plain in November 2018. Finally, we validate the model against extensive ground-based observations, focusing not only on $PM_{2.5}$ concentrations but critically on atmospheric visibility

https://doi.org/10.5194/egusphere-2026-4511
Preprint. Discussion started: 17 August 2026

(AV) and surface shortwave radiation (SSR) —two variables directly governed by aerosol optical properties.

In summary, this study advances beyond prior work on fractal aggregates in several key aspects. First, we develop the Fractal Aerosol Cluster Model (FACM), a parameterization scheme that establishes explicit analytical relationships between fractal dimension, radius of gyration, and optical/aerodynamic equivalent radii, making it readily applicable in regional climate and chemistry models. Second, for the first time, we online couple this fractal aerosol optical scheme into the WRF Chem model, enabling integrated simulations of aerosol–radiation–meteorology interactions during complex pollution episodes. Third, our simulation and validation results focuses not only on commonly examined variables such as aerosol optical depth, but specifically on atmospheric visibility (AV) —a critical environmental and safety indicator—using dense ground based observational networks to quantitatively demonstrate the improvements achieved. Finally, we evaluate the impact of fractal morphology on surface shortwave radiation (SSR) simulations, directly linking our findings to the assessment of aerosol radiative forcing, a core issue in climate research. These innovations collectively demonstrate the value of accounting for fractal geometry in both air quality forecasting and climate effect assessments.

2 Fractal Features of Aerosol Cluster and the Mechanisms in Fractal Aerosol Cluster Model

2.1 Growth Simulation and fractal dimension Calculation Method of Aerosol Cluster

Microscopic observations have shown that non-spherical aerosol particles—such as soot and black carbon—form through the random diffusion and aggregation of smaller monomeric spherules into cluster-like structures. This aggregation process can be effectively simulated using the Diffusion-Limited Aggregation (DLA) algorithm (Halsey, 2000). In this study, we apply the DLA algorithm to generate aerosol clusters across various spatial scales, following these steps (Halsey, 2000):

(1) Place an initial monomeric particle at the center of the simulation domain as the seed for cluster growth.

(2) Randomly release a second monomer (assumed to have the same diameter as the seed, a physically reasonable assumption given the consistent formation conditions of monomers) within a spherical region centered on the existing cluster, allowing it to undergo Brownian motion.

(3) If the new monomer moves beyond a prescribed maximum distance R_{max}, it is considered to have escaped and is removed; return to step (2). If it moves into a grid cell adjacent to the existing cluster, it attaches with a certain probability, forming a composite structure.

(4) Repeat steps (2) and (3) until the cluster reaches a specified number of monomers N.

Following this procedure, we obtain aerosol clusters with complex, irregular morphologies (Figure 1a–c; DLA code provided in the Supplement).

To quantify the geometry of these simulated clusters, we calculate their fractal dimension using the box-counting method (Liebovitch&Toth, 1989). The three-dimensional space enclosing the cluster is partitioned into boxes of side length l. Let N(l) denote the number of non-empty boxes that contain part of the cluster. The fractal dimension D_f is then defined as (Kenneth, 2003) :

https://doi.org/10.5194/egusphere-2026-4511
Preprint. Discussion started: 17 August 2026

$$D_f = \lim_{r \to 0} \frac{\ln N(l)}{-\ln l} \qquad \text{eq. 1}$$

For the clusters generated in this study, applying eq. (1) yields a fractal dimension of approximately **2.1** (Figure 1d), confirming their fractal nature.

It is crucial to emphasize that the fractal dimension D_f describes the scaling exponent of the cluster's mass (or number of monomers) with respect to its characteristic size, not its "embedding dimension" in three-dimensional space (i.e., the intuitive notion of "solidity" or "dimensionality"). A cluster with D_f close to 1 remains a fully three-dimensional structure, but with extremely sparse mass distribution and highly developed internal voids. This distinction is fundamental for correctly interpreting the theoretical derivations in this study.

Mathematically, the Hausdorff dimension D_f can take non-integer values less than 1 (e.g., the Cantor set, $D_f \approx 0.63$). In aerosol research, although most experimental observations report D_f values for soot aggregates in the range of 1.7–2.4 (Sorensen, 2001), highly chain-like structures with D_f close to 1 -- or even slightly below 1 -- are theoretically possible under very early nucleation stages or specific confined diffusion conditions. Our model formulation (eq. 2) is mathematically fully compatible with the cases where $D_f < 1$, demonstrating the generality and extensibility of the parameterization scheme.

It is important to note that the fractal dimension obtained from the DLA simulations ($D_f \approx 2.1$) represents the structure of freshly generated soot aggregates under ideal free-coagulation conditions, without any external compaction. However, in the real atmosphere, aerosols undergo aging processes – including condensation, coagulation, and hygroscopic growth – which gradually compact the clusters and increase their fractal dimension toward 3. For example, laboratory studies have shown that fresh soot ($D_f \approx 2.1$) can reach $D_f \approx 2.8$ after coating with sulfuric acid and exposure to high humidity (Zhang, et al., 2008). Therefore, for our case simulations over the North China Plain (winter haze, relatively aged aerosols), we adopted a representative value of $D_f = 2.7$ as a physically based engineering approximation. This choice is not inconsistent with the DLA result; rather, it reflects the more compact state of ambient aerosols.

https://doi.org/10.5194/egusphere-2026-4511
Preprint. Discussion started: 17 August 2026

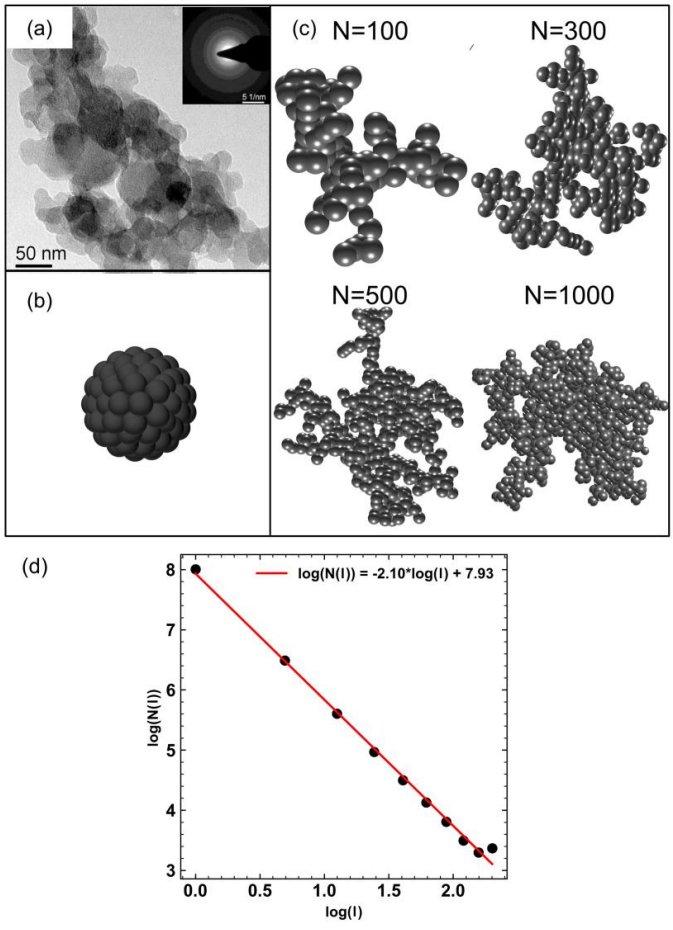

177

178 **Figure 1**. simulated fractal aerosols of different scales by DLA and calculation of their fractal dimensions

179 a: microscopy photography of an aerosol cluster (Panda&Das, 2017). b: Schematic diagram of the aerosol
180 agglomerate model. c: those simulated by the DLA to be the non-spherical fractal cluster with monomer counts
181 of 100, 300, 500, and 1000. d: the fractal dimension of non-spherical fractal cluster above by Box-counting
182 method, given by the slope of the linear fitting, side length of each three-dimensional box was denoted by l.

183 **2.2 Mathematical Principles of the Fractal Aerosol Cluster Model**

184 **Radius of gyration** (R_g)**.** Numerous observations have established that aerosol clusters can be
185 regarded as aggregates formed through the coagulation and growth of approximately homogeneous
186 spherical monomer particles.

187 The **radius of gyration**, denoted by R_g, is the characteristic measure of the overall spatial extent
188 of such a fractal aggregate. It is important to note that R_g is not intended to represent the outermost
189 boundary distance (i.e., R_{max}) of the cluster; rather, it serves as a statistical scale that describes
190 how mass is distributed around the center of mass. For a fractal cluster, the fractal dimension D_f is
191 related to R_g through a fundamental scaling law (Sorensen, 2001) :

https://doi.org/10.5194/egusphere-2026-4511
Preprint. Discussion started: 17 August 2026

$$N = k_0 \left(\frac{R_g}{a}\right)^{D_f} \quad \text{eq. 2}$$

which directly implies the power-law relationship:

$$R_g \propto N^{\frac{1}{D_f}} \quad \text{eq. 2}'$$

Here, N is the number of monomers comprising the cluster, a is the monomer radius, and k_0 is a fractal prefactor of order unity (Sorensen, 2001).

This study strictly adheres to the classical definition of R_g established in the field of light scattering by fractal aerosol aggregates (Sorensen, 2001; Heinson, et al., 2016). It should be noted that Equation (2) is an empirical scaling law in fractal scaling theory; its primary role is to reveal power-law relationships, and constant factors (such as k_0 or $\sqrt{3/5}$) do not affect the scaling exponent.The core physical implication of Eq. (2) is that the dependence of R_g on N is entirely governed by the fractal dimension D_f:

when $D_f = 3$ (compact sphere), we have $R_g \propto N^{1/3}$, consistent with the volume–scale relationship of classical three-dimensional objects.

when $D_f < 3$ (fractal object), we have $R_g \propto N^{1/D_f}$, meaning that R_g grows significantly faster with increasing N than in the compact sphere case. This accelerated growth mathematically embodies the "porous" or "fluffy" structure characteristic of fractal aggregates.

This power-law relationship serves as the logical foundation for all theoretical derivations in this study.

When a cluster grows isotropically, the distance from its center of mass to the center of an outermost monomer can be approximated by the radius of gyration R_g. This approximation is widely adopted in fractal aerosol studies (see the schematic illustration in Sorensen, 2001, Figure 4) and is justified by a clear **scale separation**: the monomer radius a is typically one to two orders of magnitude smaller than R_g (i.e., $R_g/a \sim 10^1$–10^2). Consequently, any constant factor (such as the ratio R_g/R_{max}) that arises from this approximation is independent of N and D_f and does not affect the power-law scaling exponents that are the central focus of this study.

Specifically, when the fractal dimension of the cluster is 3, the overall structure is compact, with no voids inside. At this point, for a spherical cluster, its volume $V_{sph,3}$ is given by:

$$V_{sph,3} = N \cdot \frac{4}{3}\pi a^3 \propto \frac{4}{3}\pi {R_g}^3 \quad \text{eq. 2}''$$

Thus,

$$R_g \propto a \cdot N^{\frac{1}{3}} \quad \text{eq. 2}'''$$

It confirms that the fractal dimension is the scaling exponent in the power-law relationship between the gyration Radius and the number of monomers.

The density of an aerosol cluster (ρ_{fra}): The structure of an aerosol clusters can be considered to be a composition of aggregated monomers with air-filled voids interspersed. The cluster density ρ_{fra} needs to be calculated based on the densities of the constituent monomers ρ_0 and the air ρ_{air}, weighted by the respective volume fractions they occupy within the cluster structure.

https://doi.org/10.5194/egusphere-2026-4511
Preprint. Discussion started: 17 August 2026

$$\rho_{fra} = \frac{m_{tot}}{V_{tot}} = \frac{m_m + m_{void}}{V_{tot}} = \frac{\rho_0 \cdot V_m + \rho_{air} \cdot (V_{tot} - V_m)}{V_{tot}} \quad \text{eq. 3}$$

Here, $V_{tot} = V_{void} + V_m$ denotes the total volume of an aerosol cluster, with V_{void} referring to the void volume and V_m to the material volume. V_{tot} can be expressed in terms of the gyration Radius as:

$$V_{tot} = \frac{4}{3}\pi {R_g}^3 \quad \text{eq. 4}$$

The material volume occupied by the monomers within the cluster is given by:

$$V_m = N \cdot \frac{4}{3}\pi a^3 \quad \text{eq. 5}$$

By combining eq. 3 to eq. 5, we obtain:

$$\rho_{fra} = \rho_0 \cdot \frac{a^3}{{R_g}^3} N + \rho_{air}\left(1 - \frac{a^3}{{R_g}^3} N\right) \quad \text{eq. 6}$$

By combining with eq. 2′, we can derive:

$$\rho_{fra} \propto \rho_0 \cdot {R_g}^{D_f - 3} + \rho_{air}\left(1 - {R_g}^{D_f - 3}\right) \quad \text{eq. 7}$$

$$\rho_{fra} \propto \rho_0 \cdot N^{\frac{D_f - 3}{D_f}} + \rho_{air}\left(1 - N^{\frac{D_f - 3}{D_f}}\right) \quad \text{eq. 7′}$$

By eq. 7', it is obvious that when $D_f = 3$, ρ_{fra} does not change significantly while N varies. This means that for a three-dimensional aerosol cluster, i.e., densely polymerized by monomers with almost no voids between them, the averaged density ρ_{fra} does not changed significantly with the aggregation scale of the particle size. ρ_{fra} is linearly proportional to the monomer density.

$$\rho_{fra} \propto \rho_0 \quad \text{eq. 7″}$$

While, if $D_f < 3$, assuming the overall fractal dimension of the cluster remains constant during growth, the cluster density ρ_{fra} tends toward the air density ρ_{air} as the number of monomers N increases.

In fractal clusters, a decrease in the fractal dimension corresponds to a reduced contribution of the monomer volume within the total apparent volume of the cluster. When the fractal dimension is small, the volume occupied by the monomers increases more slowly with increasing N than the apparent three-dimensional volume of the cluster. Since both ρ_0 and ρ_{air} are constants, it follows that:

$$\rho_{fra} \propto N^{\frac{D_f - 3}{D_f}} \quad \text{eq. 7‴}$$

Aerodynamic equivalent radius (R_{ae}). The aerodynamic equivalent radius R_{ae} of an aerosol is defined as the radius of a sphere with standard density ρ_{std} (1 g cm^{-3}) that exhibits the same terminal settling velocity v_{Ts} as the particle under consideration (Hinds&Zhu, 2022). By definition, during aerosol settling in air, when the particle's settling velocity reaches v_{Ts}, the gravitational force is balanced by the aerodynamic drag force:

$$m_{tot} \cdot g = F_{drag} = \frac{3\pi\eta v_\chi \cdot R}{C_c(R)} \quad \text{eq. 8}$$

https://doi.org/10.5194/egusphere-2026-4511
Preprint. Discussion started: 17 August 2026

Here, R represents the characteristic size of the particle, which in the original reference typically refers to the radius of a sphere having the same volume as the particle (i.e., the volume-equivalent radius, R_{ve}); χ is the dynamic shape factor, introduced to correct for the drag force deviation due to non-sphericity; $C_c(R)$ is the Cunningham slip correction factor; η is the dynamic viscosity of air; and v is the terminal settling velocity of the particle.

In classical aerosol mechanics, the characteristic size R in Eq. (8) is typically taken as the volume-equivalent radius R_{ve} of the particle (Hinds & Zhu, 2022). However, for clusters with fractal structures that contain substantial internal voids, the material volume is much smaller than the apparent volume, and the volume-equivalent radius cannot reflect the true spatial extent of the cluster or its interaction with the fluid. Therefore, in this study, we adopt the radius of gyration R_g as the characteristic size—a geometric parameter that not only characterizes the overall size of the cluster but also directly couples with its internal structure through the fractal dimension D_f and the number of monomers N. This approach has precedent in fractal aerosol research (Sorensen, 2001; DeCarlo et al., 2004). The core idea is to use the same set of physical quantities (ρ_{fra}, R_g) to simultaneously describe both the mass and the hydrodynamic characteristic size of the cluster, thereby establishing a clear analytical link between macroscopic settling behavior and microscopic fractal structure. Substituting $m_{tot} = \rho_{fra} \cdot (4/3)\pi R_g^3$ into Eq. (8) and retaining R_g as the characteristic size in the equation. Based on the total cluster mass m_{tot} and the empirical formula for aerosol drag force (DeCarlo, et al., 2004) in the atmosphere, further derivation yields:

$$\rho_{fra} \cdot \frac{4}{3}\pi {R_g}^3 \cdot g = \frac{3\pi\eta \cdot v_{Ts} \cdot \chi \cdot R_g}{C_c(R_g)} \qquad \text{eq. 9}$$

Here η, $C_c(R_g)$ and χ is the same as those in eq.8. For particles with irregular shapes, the dynamic shape factor is almost always greater than 1, whereas it equals 1 for spherical particles. Therefore, the terminal settling velocity v_{Ts} is given by yields expression as:

$$v_{Ts} = \frac{4\rho_{fra} \cdot g \cdot C_c(R_g)}{9\eta \cdot \chi} \cdot {R_g}^2 \qquad \text{eq. 10}$$

According to the definition of, the aerodynamic equivalent radius (R_{ae}), the following relationship holds for the corresponding equivalent spherical particle:

$$v_{Ts} = \frac{4\rho_{std} \cdot g \cdot C_c(R_{ae})}{9\eta} \cdot {R_{ae}}^2 \qquad \text{eq. 11}$$

Since v_{Ts} in eq. 10 and eq. 11 is identical, combining and simplifying the two equations yields:

$$R_{ae} = \sqrt{\frac{C_c(R_g)}{C_c(R_{ae}) \cdot \rho_{std} \cdot \chi}} \cdot {\rho_{fra}}^{\frac{1}{2}} \cdot R_g \qquad \text{eq. 12}$$

The expression under the square root in eq. 11 is assumed to be approximately constant and is thus simplified as a linear coefficient, denoted by C'''. By considering eq. $2'$and eq. $7'''$, we obtain:

$$R_{ae} \propto C'' \cdot N^{\frac{D_f - 1}{2D_f}} \text{ or } R_{ae} \propto C'' \cdot R_g^{\frac{D_f - 1}{2}} \qquad \text{eq. 13}$$

It can be observed that:

1) when $D_f = 3$, $R_{ae} \propto R_g$. In this case, the aerodynamic equivalent radius is linearly related to

https://doi.org/10.5194/egusphere-2026-4511
Preprint. Discussion started: 17 August 2026

the gyration radius.

2) when $1 < D_f < 3$, the aerodynamic equivalent radius R_{ae} increases with the gyration radius R_g, but their growth rates are not of the same order of magnitude. R_g increases at a significantly faster rate than R_{ae}.

3) in the case of $0 < D_f < 1$, an increase in the gyration radius R_g leads to a decrease in the aerodynamic equivalent radius R_{ae}. This indicates that when the fractal dimension of the cluster is sufficiently small, it typically corresponds to a situation where the monomers within the cluster are very sparsely distributed and the cluster contains many voids. As the cluster progressively grows through aggregation, its terminal settling velocity under gravity in air may even gradually decrease.

4) furthermore, in the extreme case where R_g approaches infinity and D_f approaches zero, the cluster density ρ_{fra} approaches the air density ρ_{air}. Under these conditions, the aerodynamic equivalent radius R_{ae} approaches zero, causing the aerosol cluster to remain suspended in the atmosphere despite the constituent monomer density ρ_0 being greater than the air density ρ_{air}.

Optical equivalent radius (R_{oe}). The R_{oe} of an aerosol cluster is defined as the radius of a spherical particle that exhibits the same light scattering ability as the actual particle. It depends on the particle's projected area, refractive index, and the wavelength of the incident light.

For fractal aggregates, a practical proxy for R_{oe} is the projected area equivalent diameter—the diameter of a circle having the same area as the particle's two-dimensional projection.

Studies have shown that for clusters with fractal dimension $D_f \geq 2.0$, the projected area equivalent diameter is correlated with the radius of gyration R_g (Steven N Rogak, et al., 1993). Based on this, we adopt the following approximation in this study:

$$R_{oe} \cong R_g \propto N^{\frac{1}{D_f}} \qquad \text{eq. 14}$$

Note: This approximation is based on the linear relationship between the projected area equivalent diameter and the radius of gyration of fractal aggregates. Rogak et al. (1993) demonstrated through numerical simulations and experimental measurements that, for aggregates with fractal dimension $D_f \gtrsim 2$, the projected area equivalent diameter $d_p \approx 1.4R_g$, and this proportionality coefficient exhibits weak dependence on cluster size and monomer number. In this study, to focus on the derivation of scaling exponents, the proportionality coefficient has been simplified to 1. This simplification does not affect the conclusions regarding the core scaling behavior, and its reasonableness has been indirectly supported by subsequent observational validation of visibility and radiation simulations.

This relationship reveals that, under fractal assumptions, the optical equivalent radius of aerosol clusters follows a systematic scaling with the number of monomers N, governed entirely by the fractal dimension D_f.

Then, we define the ratio γ between the optical equivalent radius R_{oe} and the aerodynamic equivalent radius.

$$\gamma = \frac{R_{oe}}{R_{ae}} \propto \frac{N^{\frac{1}{D_f}}}{N^{\frac{D_f-1}{2D_f}}} = N^{\frac{3-D_f}{2D_f}} \qquad \text{eq. 15}$$

It can be observed that when $D_f = 3$, γ is a linear factor. The ratio between the optical equivalent

https://doi.org/10.5194/egusphere-2026-4511
Preprint. Discussion started: 17 August 2026

radius and the aerodynamic equivalent radius does not vary significantly with N; their growth rates are of the same order of magnitude. When $0 < D_f < 3$, γ increases with increasing N. When the cluster exhibits fractal characteristics, as the number of aggregated monomers or the characteristic particle size increases, the optical equivalent radius increases at a faster rate than the aerodynamic equivalent radius. (According to eq. 12, the R_{ae} may even decrease). Thus, resulting in a stronger atmospheric optical scattering effect. Thus, it should be noted that in traditional spherical models, the volumetric equivalent radius and the optical/aerodynamic equivalent radius are approximately linearly related; however, in fractal models ($D_f < 3$), R_{oe} and R_{ae} are decoupled, so optical calculations must use R_{ae}, while processes such as sedimentation must use R_{oe}.

It should be emphasized that Equation (15) expresses a proportionality relationship ($\propto$) between γ and the functions of N and D_f, rather than an exact equality. The implicit proportionality constant in this equation incorporates physical quantities unrelated to the fractal dimension, such as material density, dynamic shape factor, and slip correction factor. Therefore, the absolute magnitude of γ depends not only on N and D_f but also on factors such as particle chemical composition and detailed morphological characteristics. However, the core focus of this study is how the fractal dimension D_f modifies the scaling exponent of γ with respect to N, i.e., $\log\gamma \propto \frac{3-D_f}{2D_f}\log N$. To clearly illustrate this scaling behavior, Figure 3a normalizes γ to a reference state at $D_f = 3$ and $N = 1$; in this case, the vertical axis effectively represents $\log(\gamma/\gamma_{ref})$. After this normalization, the slope of the curve for $D_f = 3$ remains zero as N increases (indicating that γ does not vary with N), while the slopes of the curves for $D_f < 3$ are strictly determined by $\frac{3-D_f}{2D_f}$. This demonstrates that for aerosol particles with fractal morphological characteristics, as the cluster grows, the enhancement of their optical properties outpaces the enhancement of their aerodynamic properties. This is the core message we wish to convey to readers through this section.

2.3 From Optical Equivalent Radius to Atmospheric Visibility

In this study, the optical equivalent radius originally derived under the spherical assumption was substituted with that based on the fractal cluster hypothesis. The related optical parameters were still assumed to follow the Mie theory. Thus, the aerosol extinction coefficient b_{ext} is obtained (Fast, Gustafson, et al., 2006)from eq. 16,

$$b_{ext}(\lambda, \mathbf{x}) = \sum_{i=1}^{i=8} Q_e(x_i, \mathbf{x})\pi r_i^2 n(r_i, \mathbf{x}) \qquad \text{eq. 16}$$

Here, $n(r_i, \mathbf{x})$ is the number concentration associated with size bin **i** (number per unit volume). In the FastJ scheme applied widely in air quality forecasting models (such as WRF-Chem, applied in this study), the sizes bin for aerosol particles were decided to be 8, and the specific size ranges corresponding to each bin i are provided in Section 3. The Q_e, the extinction efficiency, is a function of the wavelength λ and the aerosol optical equivalent radius r_i. It quantifies the ability of an aerosol particle to attenuate light by comparing its extinction cross-section to its geometric cross-section. Size parameter **x** are defined as:

$$\mathbf{x} = 2\pi r/\lambda \qquad \text{eq. 17}$$

https://doi.org/10.5194/egusphere-2026-4511
Preprint. Discussion started: 17 August 2026

The difference in optical equivalent radius will further result in discrepancies in the simulation results of the atmospheric aerosol extinction coefficient, then the atmospheric visibility based on the Koschmieder's equation (Israël, et al., 1959):

$$VIS = K/b_{ext} \qquad eq.18$$

Here, VIS represents the horizontal visibility in the atmosphere (unit: km), and K is a constant that varies with atmospheric conditions, often set to 3.912 in studies (Griffing, 1980; Ozkaynak, et al., 1985).

3 model configure and experiment design

In this study, the FACM was coupled into WRF-Chem to improve the simulation of aerosol visibility (AV). Numerical sensitivity experiments were set up to validation the improvement of AV simulation by FACM. A severe haze event over the North China Plain (NCP) from November 24th to 27th, 2018, was selected as the simulation period. The model domains, as shown in Figure 2, primarily cover the NCP. Additionally, the cities of Shenyang and Tianjin, along with their surrounding areas, were designated as higher-resolution nesting domains. Shenyang, a major industrial city, is characterized by significant particulate matter emissions from combustion processes. Tianjin, which serves as both an industrial region and a seaport, experiences visibility pollution influenced not only by dry haze but also by sea fog.

Table 1 presents the model configurations and settings used in this study, detailing the different pollution periods selected for simulation across various regions. The complex refractive indices for each aerosol species follow the default WRF-Chem settings for the RADM2/SORGAM mechanism (Schell, et al., 2001; Fast, Gustafson Jr., et al., 2006) and are kept identical between the CTR and EXP simulations. Moreover, in the Fast-J photolysis scheme used in this study, the aerosol size distribution is represented by eight fixed size bins on a logarithmic scale. The bin boundaries, defined in terms of particle diameter, are as follows: Bin 1: 0.01–0.02 μm, Bin 2: 0.02–0.04 μm, Bin 3: 0.04–0.08 μm, Bin 4: 0.08–0.16 μm; Bin 5: 0.16–0.32 μm, Bin 6: 0.32–0.64 μm, Bin 7: 0.64–1.28 μm, Bin 8: 1.28–2.56 μm. In our study, the eight size bins follow the standard Fast-J configuration (Wild et al., 2000), covering a diameter range from 0.01 μm to approximately 10 μm on a logarithmic scale. The aerosol number concentration $n(r_i, \mathbf{x})$ in each size bin is diagnosed online from the simulated mass concentrations within the SORGAM module, which explicitly accounts for emissions, gas-aerosol partitioning, coagulation, and deposition processes. This online coupling ensures that the size-resolved aerosol distribution responds dynamically to meteorological and chemical changes during the simulation.

The original WRF-Chem case settings were designated as the control group (CTR), while the case coupled with the Fractal Aerosol Cluster Model (FACM) served as the experimental group (EXP). In the radiative flux simulation experiments, an additional case with zero aerosol optical depth (AOD=0), designated as "Blank", was set to present an ideal scenario in which none aerosol radiative effects were considered in atmosphere. The Blank group employed the same meteorological initial conditions and physical parameterization schemes as the EXP and CTR groups. However, it exclusively utilized the WRF model framework without incorporating chemical processes or aerosol-radiation interactions. Both the CTR and EXP groups employed the same model configuration and initialized by the same meteorological and chemical field data. Key

https://doi.org/10.5194/egusphere-2026-4511
Preprint. Discussion started: 17 August 2026

meteorological variables, including near-surface air temperature, relative humidity, $PM_{2.5}$ mass concentrations, aerosol visibility (AV), and surface radiation fluxes, were compared between the CTR and EXP groups and validated against observations. This comparison aimed to assess the impact of aerosol particle fractal features on atmospheric optical properties.

It is important to emphasize that CTR and EXP are initialized with identical meteorological initial conditions, boundary conditions, and physical parameterization schemes. Therefore, at the start of the simulations, the meteorological fields in both experiments are the same. However, because EXP incorporates the Fractal Aerosol Cluster Model (FACM), which predicts stronger aerosol extinction due to larger optical equivalent radii, it modifies the atmospheric radiative transfer compared to CTR. This leads to a reduction in downward surface shortwave radiation in EXP (see Section 4.4 and Figure 8). The altered surface radiation affects the surface energy balance, which in turn feeds back to influence near surface temperature, boundary layer stability, turbulent mixing, and local circulations through the online coupled aerosol–radiation–meteorology feedback mechanism in WRF Chem. Consequently, differences in meteorological variables between EXP and CTR that emerge during the simulation (as shown in Figure 4) are physical feedback responses arising from the different aerosol optical properties, rather than being due to any anthropogenically differences in model configuration.

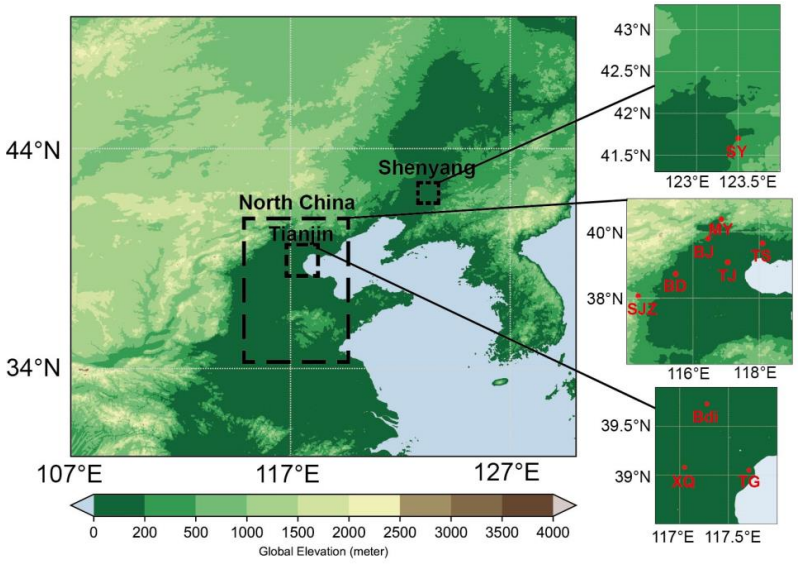

Figure 2. Model domain and the locations of urban surface meteorological observation stations (red dots): Beijing (BJ), Miyun (MY), Tianjin (TJ), Baodin (BD), Shijiazhuang (SJZ), Tangshan (TS), Shenyang (SY), Xiqing (XQ), Tanggu (TG) and Baodi (Bdi). The map in this and all following figures were entirely created by the authors. No third-party map layers were used, so no copyright statement or credit is required.

Table 1

WRF-Chem model schemes options and initial setting

schemes options

https://doi.org/10.5194/egusphere-2026-4511
Preprint. Discussion started: 17 August 2026

Long-wave radiation	RRTMG	(Iacono, et al., 2008)
Short-wave radiation	RRTMG	
Aerosol chemistry	RADM2/SORGAM	(Schell, et al., 2001)
Aerosol optical	Volume averaging mixing	
Gas chemistry	RADM2	(Stockwell, et al., 1990)
photolysis	Fast-J	(Wild, et al., 2000)
Microphysics	Purdue Lin	(S.-H. Chen&Sun, 2002)
Cumulus parameterization	Grell 3D	(Grell&Dévényi, 2002)
PBL	MYNN2	(Nakanishi&Niino, 2006)
Land-surface	Noah	(Tewari, et al., 2004)
Domain setting		
Simulated area	spatial grid	Time
North China Plain	32 km 8 km	24-27 November 2018
Tianjin	32 km 8 km 2 km	1-4 December 2023
Shenyang	32 km 8 km 2 km	13-21December 2016

For the numerical simulations in this study, an average fractal dimension of approximately 2.7 was selected, based on estimates of aerosol composition ratios in the atmosphere. But it is important to acknowledge that using the fixed fractal dimension ($D_f \approx 2.7$) is a simplification. This value was chosen as a representative estimate for the overall aerosol mixture during winter haze events in the North China Plain, based on considerations of aging processes—including compaction due to coagulation, condensation, and hygroscopic growth—that tend to increase D_f over time. While this approximation is more physically realistic than the traditional assumption of compact spheres ($D_f = 3$), it does not capture the full range of D_f variability observed under different conditions.

Observational studies has shown that the measured fractal dimension D_f of soot particles in actual atmospheric conditions typically ranges between 1.8 and 2.2 (Y. Wang, et al., 2017). However, not all aerosol particles exhibit pronounced fractal characteristics. For instance, relative humidity (RH) plays a critical role in restructuring: under high RH, hygroscopic growth can fill intra-aggregate voids or cause structural collapse, leading to an increase in effective D_f and a weakening of fractal effects. This would result in slower growth of the optical equivalent radius and reduced impacts on extinction, atmospheric visibility (AV), and surface shortwave radiation (SSR). Conversely, under dry conditions, fractal effects are more pronounced. These transformations have been documented in both laboratory experiments and field observations (Y. Wang, et al., 2017; Bai, et al., 2018) .

https://doi.org/10.5194/egusphere-2026-4511
Preprint. Discussion started: 17 August 2026

4 Results and discussion

4.1 optical radius of fractal aerosol clusters

According to the FACM theory outlined in Section 2.2, the optical properties of atmospheric aerosols are closely related to the size and fractal dimension of aerosol clusters. Figure 3 illustrates the relationship between the number of monomers N , the fractal dimension D_f and γ, the ratio of optical to aerodynamic equivalent radius. The value of γ indicates the strength of the cluster's extinction properties.

As shown in Figure 3a, an increase in N, which represents a higher number of monomers within each cluster, leads to an enhancement in the value of γ. However, when N remains constant, an aerosol cluster with a larger fractal dimension D_f—approaching a value of 3—indicates that the overall shape of the cluster is relatively symmetrical and compact, resulting in a lower γ value.

As D_f approaches 3, the variation in γ with N gradually slows and eventually converges to a constant value. In contrast, when D_f decreases, reflecting an enhancement in the fractal characteristics of the aerosol cluster, the variation in γ with N increases. This suggests that aerosol clusters with more pronounced fractal features exhibit stronger atmospheric optical effects.

As shown in Figure 3b, clusters with smaller fractal dimensions exhibit a larger discrepancy between the optical equivalent radius and the aerodynamic equivalent radius as the number of monomers increases. The lower values of fractal dimension of the particle cluster indicate more space voids within the it, resulting in larger gyration particle size in the atmosphere; while those clusters with a larger fractal dimension grow slower in gyration size and looks denser. Meanwhile, the larger gyration size and less average density of the fractal particle clusters also result in the stronger air resistance during settling and the smaller settling velocities, finally result in a smaller aerodynamically equivalent radius.
It should be noted that even for a compact sphere with $D_f = 3$, the value of γ is not equal to 1, because the material density of the particle (ρ_0) differs from the standard density ($\rho_{std} = 1\ g \cdot cm^{-3}$) used in the definition of the aerodynamic equivalent radius. In this figure, the γ value at $D_f = 3$ and $N = 1$ has been taken as the reference value γ_{ref}. Consequently, the vertical coordinate of the $D_f = 3$ curve at $N = 1$ is $\log(\gamma_{ref}) \neq 0$. However, as the core objective of this study is to reveal the influence of fractal dimension on the trend of γ with respect to N, this normalization allows us to focus on the primary physical behavior while setting aside secondary factors.

Physically, a lower fractal dimension of the particle cluster indicates the presence of more void spaces within it, leading to a larger gyration particle size in the atmosphere. In contrast, clusters with a higher fractal dimension exhibit slower growth in gyration size and appear denser. Additionally, the larger gyration size and lower average density of fractal particle clusters increase air resistance during settling, resulting in smaller settling velocities and, ultimately, a reduced aerodynamically equivalent radius. Thus, this explains why particle clusters with smaller fractal dimensions have larger γ values, which correspond to the ratio of the optical equivalent radius to the aerodynamically equivalent radius.

https://doi.org/10.5194/egusphere-2026-4511
Preprint. Discussion started: 17 August 2026

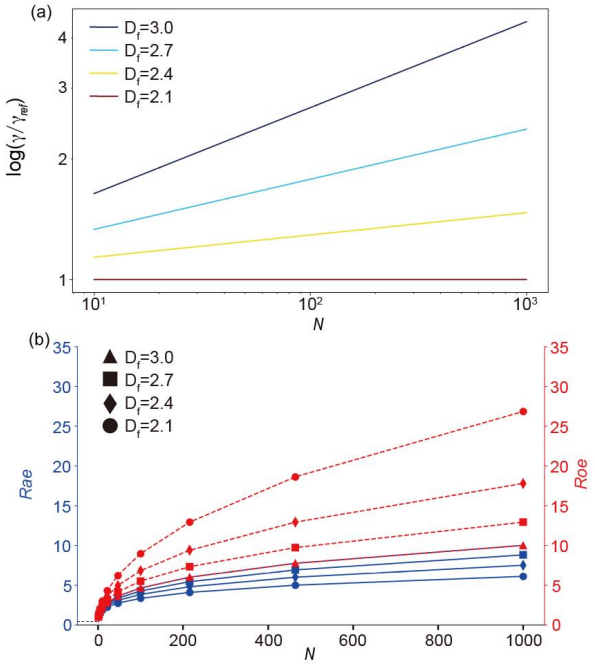

Figure 3. Relationship between the aerodynamic and optical equivalent radii as the number of monomers increases.

(a) The ratio $\gamma = \frac{R_{oe}}{R_{ae}}$ as a function of N for different fractal dimensions D_f (indicated by colors). Both axes are on a natural logarithmic scale. The values in brown are normalized to a reference state at $D_f = 3$ and $N = 1$ (γ_{ref}). Thus, the curves illustrate the relative trend and scaling exponent ($\log \gamma \propto \frac{3-D_f}{2D_f} \log N$), not the absolute magnitude of γ. Note that $\gamma \neq 1$ even for a sphere ($D_f = 3$) because the material density (ρ_0) differs from the standard density ($\rho_{std} = 1\ g \cdot cm^{-3}$) used to define R_{ae}. Normalizing to γ_{ref} isolates the effect of D_f on the growth rate of γ.

(b) Comparison of R_{ae} (blue lines) and R_{oe} (red lines) versus N. Solid lines represent R_{ae}, and dashed lines represent R_{oe}. Different marker shapes correspond to different fractal dimensions D_f, as in panel (a).

4.2 Comparison and validation of meteorological elements.

Six cities located in the North China Plain—Beijing (BJ), Miyun (MY), Tianjin (TJ), Tangshan (TS), Baoding (BD), and Shijiazhuang (SJZ)—along with Shenyang (SY), an industrial city in Northeast China, were selected for simulation validation using observational data from stations in each city. Additionally, three monitoring stations in and near Tianjin—Baodi (Bdi), Xiqing (XQ), and Tanggu (TG)—provided supplementary observations.

As shown in Figure 4, the time series of 2-meter temperature (T2), 10-meter wind speed (WS), surface relative humidity (RH), and $PM_{2.5}$ mass concentrations from these stations were compared against simulation results from EXP and CTR. Statistical analyses of simulation errors for the aforementioned variables were conducted, and the results are summarized in Table 2.

https://doi.org/10.5194/egusphere-2026-4511
Preprint. Discussion started: 17 August 2026

As shown in Figure 4, the simulated time series of T2, WS, RH, and $PM_{2.5}$ mass concentrations in both EXP and CTR align well with the observational data. As explained in Section 3, the meteorological differences between EXP and CTR shown in Figure 4 arise from the online aerosol–radiation–meteorology feedback triggered by the FACM scheme, rather than from any differences in initial conditions or model setup. Therefore, both EXP and CTR effectively capture the meteorological conditions and temporal variations in mass concentrations during the simulation period without notable discrepancies. These results demonstrate that WRF-Chem provides a reasonable and reliable baseline simulation for the subsequent analyses in this study.

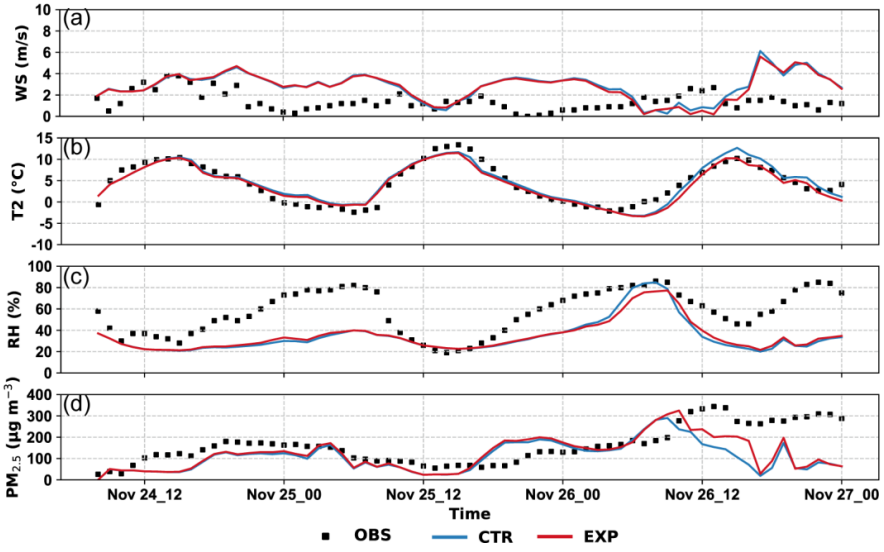

Figure 4. Time series of simulated and observed WS (a), T2 (b), RH (c), and near-ground $PM_{2.5}$ mass concentration (d) at the Beijing station. The black squares dots represent observations, the blue lines represent the simulation by CTR, and the red for EXP.

Table 2

T2, WS, RH and mass concentration of $PM_{2.5}$ in CTR to the observation.

Variables	Stations	NME(%)	NMB(%)	RMSE
T2 (°C)	BJ	28.84	3.19	1.57
	MY	144.93	46.75	4.24
	TJ	33.89	18.03	2.54
	BD	103.22	100.16	3.42
	TS	58.08	40.00	2.45
	SJZ	46.76	39.99	3.52
WS (m/s)	BJ	126.17	100.80	2.10
	MY	185.35	161.13	2.27
	TJ	70.71	63.21	1.57
	BD	120.67	111.83	1.89
	TS	83.81	75.13	1.59
	SJZ	173.61	149.29	3.57
RH (%)	BJ	41.29	-40.70	28.46
	MY	49.16	-47.38	35.87
	TJ	41.19	-41.19	36.64
	BD	103.22	100.16	3.41
	TS	39.95	-39.96	35.96

https://doi.org/10.5194/egusphere-2026-4511
Preprint. Discussion started: 17 August 2026

	SJZ	58.11	-57.84	36.17
$PM_{2.5}(\mu g/m^3)$	BJ	47.92	-32.12	103.99
	MY	66.34	-65.88	124.27
	TJ	44.55	-36.04	106.26
	BD	51.18	-50.89	160.99
	TS	51.33	-44.26	117.37
	SJZ	71.74	-71.74	157.15

Note. normalized mean error (NME), normalized mean bias (NMB) and root mean square error (RMSE)

4.3 Near-ground Horizontal Distribution of Atmospheric Visibility

4.3.1 North China Plain Case

Figure 5 presents the simulated and observed near-ground atmospheric visibility (AV) over the North China Plain (NCP) during the severe winter haze event of November 24–27, 2018. Observation stations are marked as circles, with observed AV values shown inside the circles and simulated values outside.

Throughout the haze event, observed AV remained below 5 km at most stations, dropping to less than 0.5 km during peak pollution episodes at sites such as Beijing (BJ) and Tianjin (TJ). The CTR simulation (original WRF-Chem) significantly overestimated AV, with values averaging 3–10 times higher than observations (Figure 5a–d and blue line in Figure 5i). In contrast, the EXP simulation (FACM-coupled WRF-Chem) showed markedly better agreement, both in the spatial distribution at representative moments (Figure 5e–h) and in the temporal evolution at the Beijing station (Figure 5i, red line).

Notably, both CTR and EXP successfully captured the spatial and temporal patterns of PM2.5 mass concentrations (Figure 4), indicating that the improvement in AV simulation by EXP stems directly from its consideration of fractal aerosol morphology and its impact on optical properties, rather than from differences in mass concentration predictions.

Despite the non-negligible meteorological and $PM_{2.5}$ concentration biases shown in Figure 4, the visibility simulations in both CTR and EXP are affected by these biases in a symmetric manner – because the two experiments share identical meteorological fields, emission inventories, and chemical mechanisms. Consequently, the systematic difference between EXP and CTR (the red vs. blue lines in Figure 5i) can be unambiguously attributed to the FACM optical modification. Notably, EXP consistently yields lower (i.e., more realistic) visibility values than CTR across all periods, and this improvement is large enough to be discernible even when the absolute simulation errors are substantial. Thus, the meteorological biases do not undermine the robustness of our conclusion that accounting for fractal geometry significantly improves visibility simulations.

4.3.2 Tianjin Region: Coastal Influence

To further investigate the role of fractal morphology under different aerosol regimes, we conducted sensitivity simulations for the Tianjin region, which includes both inland and coastal stations (Baodi, Xiqing, and Tanggu; Figure 6).

As shown in Figure 6, EXP consistently outperformed CTR in simulating AV across all three stations. However, the degree of improvement varied systematically with distance from the coast. At Tanggu (TG), located only 10 km from the coastline, the CTR simulation already showed reasonable agreement with observations, and the improvement by EXP was relatively modest (Figure 6i). This can be attributed to the high humidity and sea-salt aerosol content characteristic

https://doi.org/10.5194/egusphere-2026-4511
Preprint. Discussion started: 17 August 2026

of coastal environments, which promote hygroscopic growth and lead to more spherical particle shapes—conditions under which the spherical aerosol assumption in CTR remains reasonably valid.

In contrast, at Xiqing (XQ, ~50 km inland) and Baodi (Bdi, >70 km inland), the improvement by EXP became progressively more pronounced. As distance from the coast increases, the influence of marine aerosols diminishes, and the aerosol population becomes increasingly dominated by anthropogenic emissions with pronounced fractal morphologies. Consequently, the CTR simulation increasingly overestimates visibility, while FACM effectively captures the enhanced extinction due to fractal structure.

We did not screen visibility observations for hydrometeors (fog, cloud, drizzle) because the objective was to compare CTR and EXP under real atmospheric conditions. However, future studies aiming to isolate pure aerosol effects should apply such screening (e.g., using RH thresholds, cloud cover, precipitation records).

4.3.3 Shenyang: Industrial Emissions Case

Shenyang (SY), located in one of China's largest heavy industrial regions, provides an additional test case dominated by anthropogenic combustion emissions—precisely the type of aerosol for which fractal morphology is most pronounced.

During the selected winter pollution episode, the CTR simulation severely overestimated AV, with deviations reaching 10–20 times the observed values (Figure 7a–d, blue line in Figure 7i). In contrast, EXP achieved dramatically improved agreement, with the simulated visibility closely matching observations, especially during the peak pollution period from December 19 to 21 (Figure 7e–h, red line in Figure 7i).

The exceptional improvement in Shenyang—exceedingly even that seen in the North China Plain case—underscores that FACM delivers the greatest benefit in environments dominated by fresh, fractal-rich anthropogenic emissions, while its impact is more limited in regions where hygroscopic or naturally spherical aerosols prevail.

4.3.4 Summary of Visibility Improvements

Table 3 summarizes the statistical performance of CTR and EXP across all 10 validation stations. The average normalized mean error (NME) for AV was reduced from 421.62% in CTR to 163.39% in EXP—a substantial relative improvement. However, the remaining absolute error is still considerable, and further refinements are needed. Therefore, we conclude that FACM provides a significant improvement over the spherical assumption, while acknowledging that residual uncertainties remain.

https://doi.org/10.5194/egusphere-2026-4511
Preprint. Discussion started: 17 August 2026

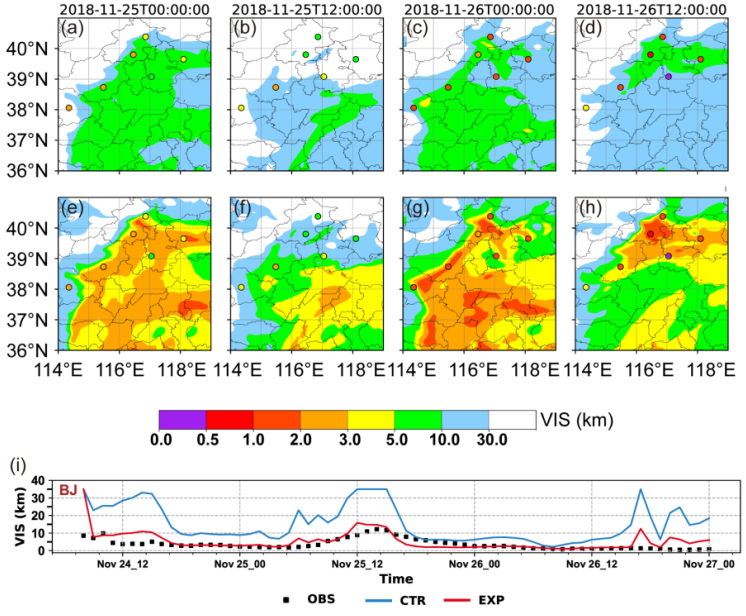

Figure 5. Observed and simulated near-ground distributions of AV over NCP, and the AV timeseries at station BJ. The subplot a-d show the simulation by CTR at four typical moments, the subplots e-h for EXP, simulation time is displayed as local time (UTC +8); subplot i illustrates the timeseries of AV at station BJ: the black square

https://doi.org/10.5194/egusphere-2026-4511
Preprint. Discussion started: 17 August 2026

markers (OBS) represent the observed at BJ; the blue line (CTR) stands for other by CTR and the red line (EXP) by EXP simulation.

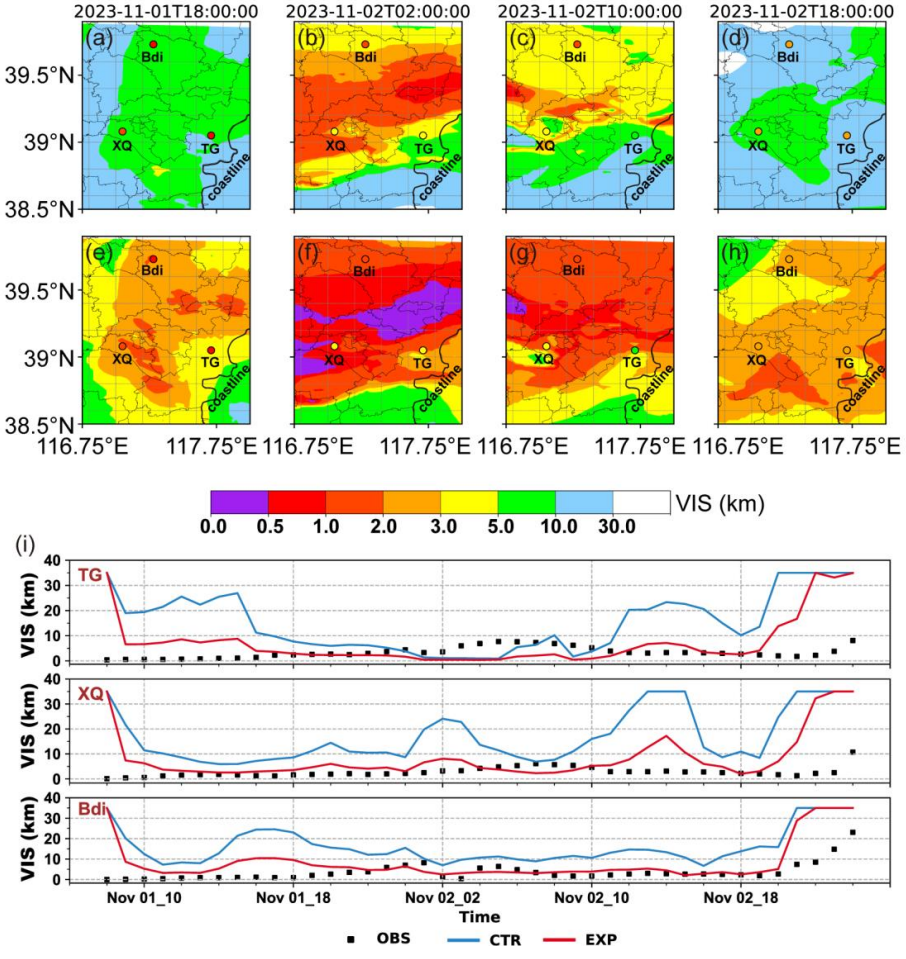

Figure 6. observed and simulated near-ground distributions of AV over Tianjin, and the AV timeseries at station TG, XQ and Bdi. The subplot a-d show the simulation by CTR at four typical moments, the subplots e-h for EXP, simulation time is displayed as local time (UTC +8); subplot i illustrates the timeseries of AV at

https://doi.org/10.5194/egusphere-2026-4511
Preprint. Discussion started: 17 August 2026

station TG, XQ and Bdi: the black square markers (OBS) represent the observation; the blue line (CTR) stands for other by CTR and the red line (EXP) by EXP simulation.

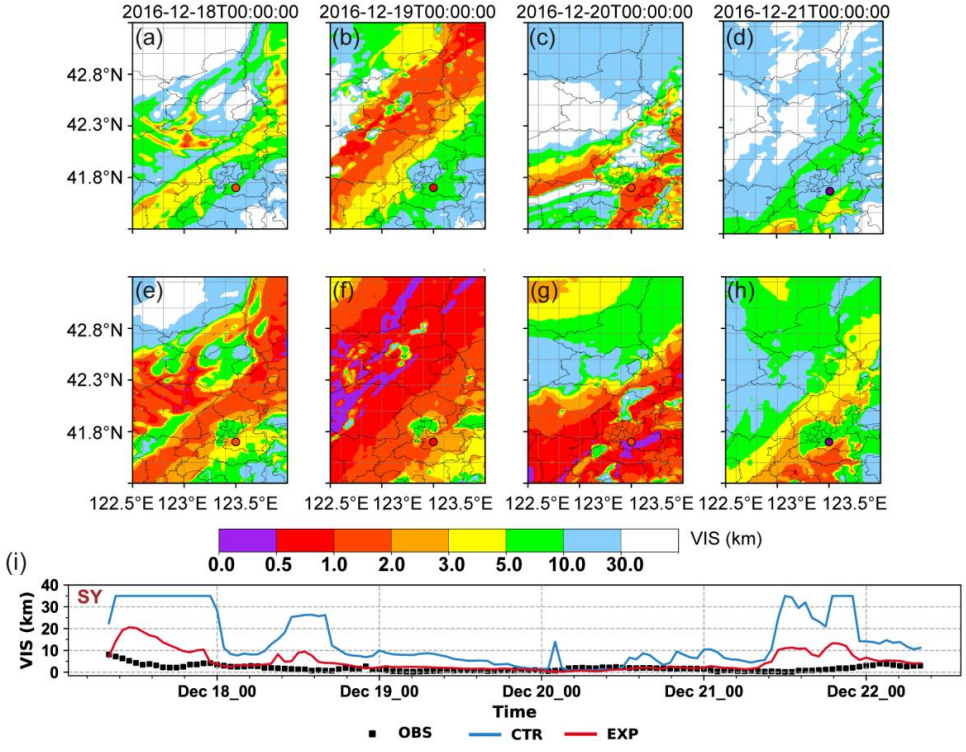

Figure 7. observed and simulated near-ground distributions of AV over Shenyang, and the AV timeseries at station SY. The subplot a-d show the simulation by CTR at four typical moments, the subplots e-h for EXP, simulation time is displayed as local time (UTC +8); subplot i illustrates the timeseries of AV at station SY: the black square markers (OBS) represent the observation; the blue line (CTR) stands for other by CTR and the red line (EXP) by EXP simulation.

The cross-regional comparison reveals a consistent pattern: the improvement by FACM is most pronounced in environments with high proportions of fresh anthropogenic emissions (Shenyang, inland Tianjin), moderate in mixed urban-industrial regions (North China Plain), and least in coastal areas where hygroscopic aerosols approach spherical shapes (Tanggu). This gradient provides strong evidence that the fractal morphology of aerosol particles is a first-order factor governing their optical effects, and that FACM successfully captures this relationship.

4.4 Influence of Fractal Aerosol Clusters on the Surface Shortwave Radiation Budget

The influence of fractal aerosol geometry extends beyond atmospheric visibility to directly impact the surface energy balance. By altering the extinction of solar radiation as it traverses the atmosphere, the fractal structure of aerosol clusters modulates the amount of shortwave radiation reaching the ground.

https://doi.org/10.5194/egusphere-2026-4511
Preprint. Discussion started: 17 August 2026

627 Figure 8 presents the simulated daily mean surface shortwave radiation (SSR) from EXP (a), CTR
628 (b), and the "Blank" (c, aerosol-free) experiments, along with their differences. It is important to
629 clarify that the FACM correction applies to all aerosol species exhibiting fractal morphology (not
630 only black carbon); therefore, the difference shown in Figure 8d (EXP–CTR) represents the
631 additional radiative forcing due to the morphological correction, rather than the 'black carbon
632 effect alone. The key results are threefold. First, the inclusion of fractal morphology leads to a
633 substantial reduction in SSR. The domain-averaged SSR in EXP is approximately 30 $W \cdot m^{-2}$ lower
634 than in CTR, with localized reductions of 40–60 $W \cdot m^{-2}$ in and around urban areas (Figure 8d).
635 Second, this reduction is comparable in magnitude to the total aerosol effect itself (CTR vs. Blank,
636 Figure 8e), underscoring that particle morphology is a first-order factor in aerosol-radiation
637 interactions. Third, and most importantly, the EXP simulation shows significantly better
638 agreement with hourly SSR observations at the Beijing station (Figure 8f) than CTR, particularly
639 during peak haze periods when SSR is lowest.

640 This observational validation is critical. It confirms that the stronger shortwave attenuation
641 predicted by FACM is not an artifact, but a physically realistic correction to the systematic
642 overestimation inherent in traditional spherical aerosol models (CTR). By more accurately
643 representing the extinction properties of fractal clusters—especially those dominated by
644 anthropogenic soot—FACM provides a more faithful simulation of the surface radiative cooling
645 effect during heavy haze episodes.

646 These findings demonstrate that accounting for fractal aerosol morphology is essential for reliable
647 simulations of surface radiation and, by extension, for assessing the climatic impacts of
648 anthropogenic aerosols.

649 **Table 3**

650 Statistical analysis of AV by sensitivity simulation for each station in this study.

Stations	NME (%)		NMB (%)		RMSE	
	CTR	EXP	CTR	EXP	CTR	EXP
BJ	319.30	71.52	319.30	48.03	14.45	4.59
MY	398.73	215.05	398.73	214.90	21.69	15.94
TJ	168.82	77.40	151.18	-10.05	10.58	5.70
BD	411.67	91.30	411.68	74.85	11.95	4.62
TS	225.28	122.14	225.29	46.22	15.00	9.49
SJZ	739.25	291.33	739.25	288.11	24.32	12.45
TG	396.03	199.34	396.03	114.41	17.13	10.91
XQ	517.15	225.52	517.15	203.12	17.53	10.62
Bdi	347.54	153.90	347.54	153.90	14.37	9.27
SY	692.43	186.40	685.20	172.63	16.73	5.26
average	**421.62**	**163.39**	**419.135**	**130.612**	**16.375**	**8.885**

651

https://doi.org/10.5194/egusphere-2026-4511
Preprint. Discussion started: 17 August 2026

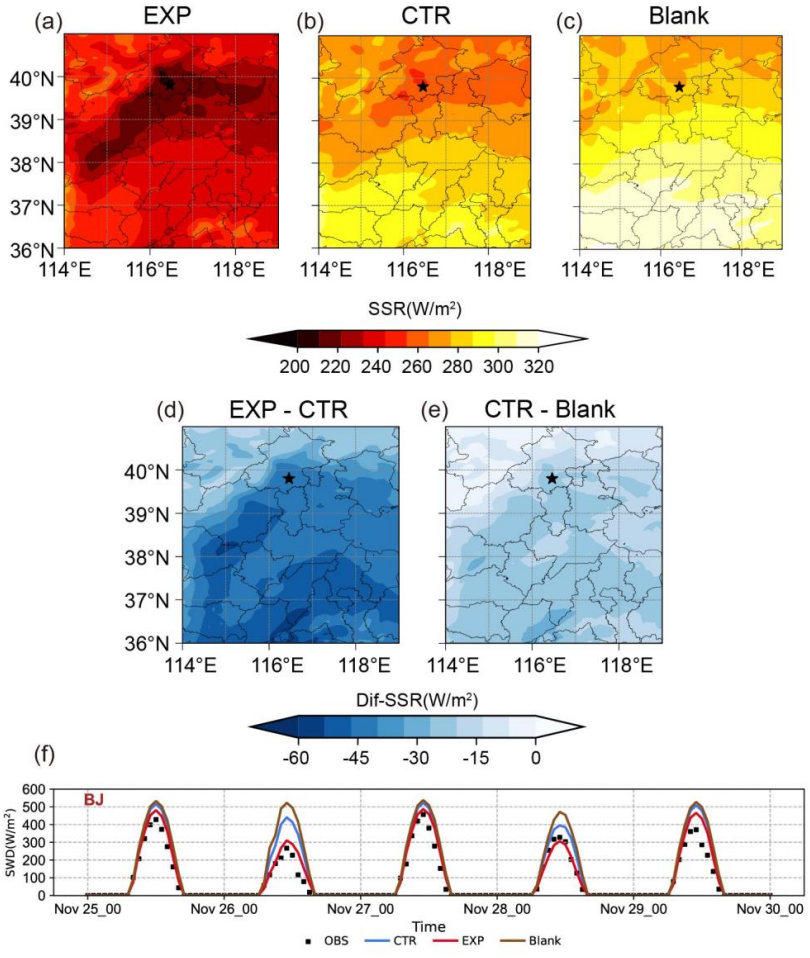

Figure 8. Daily Averaged Downwards Surface Shortwave Radiation (SSR) distribution over North China by simulation (a. EXP; b. CTR; c. Blank d. EXP-CTR; e. CTR-Blank) and the hourly timeseries of simulated and observed SSR at the Beijing station (f). the black square markers (OBS) represent the observation; the blue line (CTR) stands for other by CTR; the brown line (Blank) stands for other by Blank and the red line (EXP) by EXP simulation.

4.5 Applicability of FACM to Different Aerosol Regimes

While this study focuses on a soot rich haze episode, it is important to consider the applicability of the Fractal Aerosol Cluster Model (FACM) to other aerosol regimes. The FACM is expected to yield the most significant improvements for pollution events dominated by anthropogenic emissions, particularly fossil fuel and biomass burning, under relatively dry atmospheric conditions. In such cases—exemplified by our main study case over the North China Plain and the Shenyang industrial episode—aerosols such as soot and black carbon exhibit pronounced fractal morphologies, and accounting for their fractal structure substantially improves visibility and radiation simulations.

https://doi.org/10.5194/egusphere-2026-4511
Preprint. Discussion started: 17 August 2026

In contrast, for regimes dominated by mineral dust or high humidity sulfate episodes, the improvements offered by FACM are likely to be more limited. Mineral dust particles are irregular in shape but generally compact, with less pronounced fractal characteristics; existing non spherical models (e.g., ellipsoidal representations) may be more appropriate, although FACM could still be tested as an alternative approach. Under high relative humidity (RH), sulfate and other hygroscopic aerosols undergo substantial water uptake, becoming near spherical droplets. In such cases, traditional spherical assumptions with appropriate hygroscopic growth corrections may suffice, as suggested by the relatively modest improvement at the coastal Tanggu station compared to inland sites in our study (see Section 4.3).

Therefore, while FACM provides a robust framework for fractal carbonaceous aerosols, its application to other aerosol types should be evaluated carefully. Future work should focus on developing morphology dependent parameterizations that can seamlessly transition between fractal, compact non spherical, and near spherical representations depending on aerosol composition, age, and ambient RH.

5. Conclusion

In this study, a growth model for aerosol clusters based on the Diffusion-Limited Aggregation (DLA) algorithm was first applied to simulate the aggregation process of smaller monomeric particles into clusters. It was demonstrated that the aerosol clusters exhibit fractal geometric characteristics, supported by a cluster of previous observation studies. Then the fractal dimensions of the clusters were calculated by the box-count method, and the optical and aerodynamically equivalent radii of the fractal aerosol clusters were analyzed, proving that they are determined by both the fractal dimension and the size of the clusters. Then these results were parameterized to qualify how the fractal morphology of the aerosol particles influence the atmospheric optical in Fractal Aerosol Cluster Model (FACM). Finally, FACM was coupled into WRF-Chem, and sensitivity numerical experiments were conducted, with station observations used for validation. The results for atmospheric visibility and surface shortwave radiation flux demonstrated the superior performance of EXP compared to CTR. The main findings of this study are as follows:

1. The irregular shapes of the aerosol particles found in previous microscopic observations were found to exhibit fractal characteristics, and it was demonstrated that the fractal dimension of aerosol particles influences their optical and aerodynamic equivalent radii. The FACM model was established and used to show that a value of fractal dimension lower than 3 can lead to a greater ratio of optical equivalent radius to aerodynamic equivalent radius, which in turn results in a higher atmospheric extinction coefficient and lower atmospheric visibility.
2. By coupling FACM into WRF-Chem, the impact of aerosol fractal characteristics on atmospheric optical properties was confirmed through numerical sensitivity experiments and observational validation. The results from EXP significantly improved the simulation accuracy of WRF-Chem for atmospheric visibility. For instance, the Normalized Mean Error (NME) at the Beijing station decreased from 319.3% in the CTR group to 71.52% in the EXP group. At the Tanggu, Xiqing, and Baodi stations in Shenyang, the average NME decreased from 420.24% in the CTR group to 192.92% in the EXP group. The NME at the Shenyang station decreased from 692.43% in the CTR group to 186.40% in the EXP group.
3. The influence of aerosol fractal characteristics on atmospheric optical properties also affects the downward shortwave radiation budget at the Earth's surface. By coupling FACM into

https://doi.org/10.5194/egusphere-2026-4511
Preprint. Discussion started: 17 August 2026

WRF-Chem, the simulated downward SSR flux results show significant improvement compared to the original model, reducing the overestimation observed in the CTR simulations. Moreover, the improvement brought by FACM is more pronounced during pollution episodes and in areas dominated by anthropogenic emissions, while the improvement is less significant during periods and in areas dominated by natural emissions and hygroscopic aerosols. Crucially, the enhanced SSR simulations in EXP have been validated against observational data (Figure 8f), confirming that the stronger extinction by fractal aerosol clusters leads to a more realistic representation of surface radiative forcing. This observational validation underscores the physical reasonableness of the FACM framework and its value for improving climate effect assessments. These findings demonstrate that accounting for fractal geometry can substantially improve visibility and radiation simulations, and also provide valuable insights for future research on aerosol radiative forcing in the context of global and regional climate changes.

However, this research requires further development in the future:

1. The fractal characteristics of aerosol particles, including their fractal dimension and particle size distribution, vary significantly across different sources and formation processes under complex atmospheric conditions. By using a fixed $D_f \approx 2.7$, our current approach may **underestimate** the enhancement of extinction in very dry, fresh-soot-dominated scenarios, while potentially **overestimating** fractal effects in high-RH, hygroscopic-aerosol-dominated conditions. In future work, we plan to develop a more sophisticated parameterization that accounts for the dependence of D_f on aerosol composition, age, and RH, enabling a more accurate representation of fractal morphology under varying atmospheric conditions.
2. It should be noted that this study employs the simplifying assumption $R_{oe} \cong R_g$ when defining the optical equivalent radius. This assumption is primarily based on the classic conclusion that the projected area equivalent diameter of fractal aggregates is approximately proportional to the radius of gyration (Steven N. Rogak, et al., 2007), and its applicability within the framework of this study has been indirectly validated by comparing simulation results with multi-site visibility and radiation observations. However, for aggregates with low fractal dimensions ($D_f \lesssim 1.8$) or highly asymmetric structures, the error associated with this approximation may increase. Future work will introduce more refined parameterization schemes for the optical equivalent radius, such as establishing multidimensional lookup tables for R_{oe} as a function of R_g, D_f, and refractive index based on the Discrete Dipole Approximation (DDA) or T-matrix methods, to further enhance the generality and accuracy of the model. In this study, the fractal dimension was approximated as a constant, which is considered a reasonable assumption, but this approach will be refined in future research.
3. The considerable absolute errors of VIS and radiation budget remain. Further work is required to address residual uncertainties.

https://doi.org/10.5194/egusphere-2026-4511
Preprint. Discussion started: 17 August 2026

Author Contribution Statement

Zhenxin Liu: Funding acquisition, Conceptualization; Methodology; Model Development; Writing & Manuscript revision; Visualization and Validation; **Li Weimin:** Model coding and running; Visualization and Validation; **Zhang Bihui**: Observation data & draft revision; **Yuhao Mao**: Methodology & Draft revision. **Ma Xinye**: figure plotting & Visualization advices; **Zhang kuan**: Model coding and running; Initial Writing; **Hong Liao**: Funding acquisition

Declaration of competing interest

The authors declare that they have no known competing financial interests or personal relationships that could have appeared to influence the work reported in this paper.

Acknowledgments

We acknowledge the High-Performance Computing Centre of Nanjing University of Information Science and Technology for their support of this work.

Financial support

This work was supported by Jing-Jin-Ji Regional Integrated Environmental Improvement-National Science and Technology Major Project (2025ZD1201601) and the Natural Science Foundation of Liaoning Province (No. 2024-MS-245).

Data and Codes Availability Statement

The National Centers for Environmental Prediction Global Final Analysis (NCEP-FNL) data is available at (National Centers for Environmental Prediction, 2015). The input data for WRF-Chem simulations, as well as the observational and simulated meteorological and air quality data for validation and analysis in this study, are available at (Z. Liu, et al., 2024). The DLA and FACM source codes, along with the configuration, initialization, and output files for the WRF-Chem-FACM simulations, are available at (Z. Liu, et al., 2025).

References

Bai, Z., Ji, Y., Pi, Y., *et al.* (2018). Hygroscopic analysis of individual Beijing haze aerosol particles by environmental scanning electron microscopy. *Atmospheric Environment, 172*, 149-156. doi:10.1016/j.atmosenv.2017.10.031

Che, H., Zhang, X., Li, Y., *et al.* (2007). Horizontal visibility trends in China 1981–2005. *Geophysical research letters, 34*(24). doi:10.1029/2007GL031450

Chen, G., Liu, C., Wang, J., *et al.* (2024). Accounting for black carbon mixing state, nonsphericity, and heterogeneity effects in its optical property parameterization in a climate model. *Journal of Geophysical Research: Atmospheres, 129*(16), e2024JD041135.

Chen, S.-H., & Sun, W.-Y. (2002). A one-dimensional time dependent cloud model. *Journal of the Meteorological Society of Japan. Ser. II, 80*(1), 99-118. doi:10.2151/jmsj.80.99

DeCarlo, P., Slowik, J., Worsnop, D., *et al.* (2004). Particle Morphology and Density Characterization by Combined Mobility and Aerodynamic Diameter Measurements. Part 1: Theory. *Aerosol Science and Technology, 38*(12), 1185-1205.

E., A., & M., K. (2015). Coupling aerosol optics to the chemical transport model MATCH (v5.5.0) and aerosol dynamics module SALSA (v1). *Geoscientific Model Development Discussions, 8*(12), 10735-10781.

https://doi.org/10.5194/egusphere-2026-4511
Preprint. Discussion started: 17 August 2026

Fast, J. D., Gustafson Jr., W. I., Easter, R. C., *et al.* (2006). Evolution of ozone, particulates, and aerosol direct radiative forcing in the vicinity of Houston using a fully coupled meteorology-chemistry-aerosol model. *Journal of Geophysical Research: Atmospheres, 111*(D21). doi:https://doi.org/10.1029/2005JD006721

Grell, G. A., & Dévényi, D. (2002). A generalized approach to parameterizing convection combining ensemble and data assimilation techniques. *Geophysical research letters, 29*(14), 38-31-38-34. doi:10.1029/2002GL015311

Griffing, G. W. (1980). Relations between the prevailing visibility, nephelometer scattering coefficient and sunphotometer turbidity coefficient. *Atmospheric Environment (1967), 14*(5), 577-584. doi:10.1016/0004-6981(80)90089-X

Halsey, T. C. (2000). Diffusion-limited aggregation: A model for pattern formation. *Physics Today, 53*(11), 36-41. doi:10.1063/1.1333284

Heinson, W. R., Liu, P., & Chakrabarty, R. K. (2016). Fractal scaling of coated soot aggregates. *Aerosol Science and Technology, 51*(1), 12-19. doi:10.1080/02786826.2016.1249786

Hinds, W. C., & Zhu, Y. (2022). *Aerosol technology: properties, behavior, and measurement of airborne particles*: John Wiley & Sons.

Iacono, M. J., Delamere, J. S., Mlawer, E. J., *et al.* (2008). Radiative forcing by long-lived greenhouse gases: Calculations with the AER radiative transfer models. *Journal of Geophysical Research: Atmospheres, 113*(D13). doi:10.1029/2008JD009944

Ishimoto, H., Kudo, R., & Adachi, K. (2019). A shape model of internally mixed soot particles derived from artificial surface tension. *Atmospheric Measurement Techniques, 12*(1), 107-118. doi:10.5194/amt-12-107-2019

Israël, H., Kasten, F., Israël, H., *et al.* (1959). *Koschmieders theorie der horizontalen sichtweite*: Springer.

Kenneth, F. (2003). *Fractal Geometry:Mathematical Foundations and Applications*: John Wiley & Sons, Ltd.

Liebovitch, L. S., & Toth, T. (1989). A fast algorithm to determine fractal dimensions by box counting. *physics Letters A, 141*(8-9), 386-390. doi:10.1016/0375-9601(89)90854-2

Liu, C. (2019). Optical properties of black carbon aggregates. *Springer series in light scattering: volume 3: radiative transfer and light scattering*, 167-218. doi:10.1007/978-3-030-03445-0_5

Liu, Z., Zhang, K., & Mao, Y. (2025). *DLA and FACM Codes and WRF-Chem-FACM Configuration and Output Files for "Fractal Geometry of Aerosol Particles..."*. Retrieved from: https://zenodo.org/record/14213338

Liu, Z., Zhang, K., Zhang, B., *et al.* (2024). *Data for "Fractal Geometry of Aerosol Particles and Its Impact on Atmospheric Optical Properties: Development and Validation of the Fractal Aerosol Cluster Model in a Heavy Haze Event"*. Retrieved from: https://zenodo.org/record/10875363

Mie, G. (1908). Beiträge zur Optik trüber Medien, speziell kolloidaler Metallösungen. *Annalen der Physik, 330*(3), 377-445. doi:10.1002/andp.19083300302

Mishchenko, M. I., Travis, L. D., & Mackowski, D. W. (1996). T-matrix computations of light scattering by nonspherical particles: A review. *Journal of Quantitative Spectroscopy and Radiative Transfer, 55*(5), 535-575. doi:10.1016/0022-4073(96)00002-7

Nah, T., Guo, H., Sullivan, A. P., *et al.* (2018). Characterization of aerosol composition, aerosol acidity, and organic acid partitioning at an agriculturally intensive rural southeastern US site. *Atmospheric Chemistry and Physics, 18*(15), 11471-11491. doi:10.5194/acp-18-11471-2018

Nakanishi, M., & Niino, H. (2006). An improved Mellor–Yamada level-3 model: Its numerical stability and application to a regional prediction of advection fog. *Boundary-Layer Meteorology, 119*, 397-407. doi:10.1007/s10546-005-9030-8

National Centers for Environmental Prediction, N. W. S. N. U. S. D. o. C. (2015). *NCEP GDAS/FNL 0.25 Degree Global Tropospheric Analyses and Forecast Grids*. Retrieved from: https://doi.org/10.5065/D65Q4T4Z

Ozkaynak, H., Schatz, A. D., Thurston, G. D., *et al.* (1985). Relationships between aerosol extinction coefficients derived from airport visual range observations and alternative measures of airborne particle mass. *Journal of the Air Pollution Control Association, 35*(11), 1176-1185. doi:10.1080/00022470.1985.10466020

Panda, U., & Das, T. (2017). Micro-structural analysis of individual aerosol coarse particles during different seasons at an eastern coastal site in India. *Atmospheric Pollution Research, 8*(1), 196-207. doi:10.1016/j.apr.2016.08.012

Rogak, S. N., Flagan, R. C., & Nguyen, H. V. (2007). The Mobility and Structure of Aerosol Agglomerates. *Aerosol Science and Technology, 18*(1), 25-47. doi:10.1080/02786829308959582

Romshoo, B., Müller, T., Pfeifer, S., *et al.* (2021). Optical properties of coated black carbon aggregates: numerical simulations, radiative forcing estimates, and size-resolved parameterization scheme. *Atmos. Chem. Phys., 21*(17), 12989-13010. doi:10.5194/acp-21-12989-2021

https://doi.org/10.5194/egusphere-2026-4511
Preprint. Discussion started: 17 August 2026

Schell, B., Ackermann, I. J., Hass, H., *et al.* (2001). Modeling the formation of secondary organic aerosol within a comprehensive air quality model system. *Journal of Geophysical Research: Atmospheres, 106*(D22), 28275-28293. doi:https://doi.org/10.1029/2001JD000384

Sorensen, C. M. (2001). Light Scattering by Fractal Aggregates: A Review. *Aerosol Science and Technology, 35*(2), 648-687. doi:10.1080/02786820117868

Stockwell, W. R., Middleton, P., Chang, J. S., *et al.* (1990). The second generation regional acid deposition model chemical mechanism for regional air quality modeling. *Journal of Geophysical Research: Atmospheres, 95*(D10), 16343-16367. doi:10.1029/JD095iD10p16343

Strawa, A. W., Drdla, K., Ferry, G. V., *et al.* (1999). Carbonaceous aerosol (soot) measured in the lower stratosphere during POLARIS and its role in stratospheric photochemistry. *Journal of Geophysical Research: Atmospheres, 104*(D21), 26753-26766. doi:https://doi.org/10.1029/1999JD900453

Tewari, M., Chen, F., Wang, W., *et al.* (2004). *Implementation and verification of the unified Noah land-surface model in the WRF model [presentation]*.

Tiwari, S., Kumar, R., Tunved, P., *et al.* (2016). Significant cooling effect on the surface due to soot particles over Brahmaputra River Valley region, India: An impact on regional climate. *Science of the Total Environment, 562*, 504-516. doi:10.1016/j.scitotenv.2016.03.157

Veghte, D. P., & Freedman, M. A. (2014). Facile Method for Determining the Aspect Ratios of Mineral Dust Aerosol by Electron Microscopy. *Aerosol Science and Technology, 48*(7), 715-724. doi:10.1080/02786826.2014.920484

von Hoyningen-Huene, W., & Posse, P. (1997). Nonsphericity of aerosol particles and their contribution to radiative forcing. *Journal of Quantitative Spectroscopy and Radiative Transfer, 57*(5), 651-668. doi:10.1016/S0022-4073(96)00153-7

Wagh, S., Kulkarni, R., Lonkar, P., *et al.* (2023). Development of visibility equation based on fog microphysical observations and its verification using the WRF model. *Modeling Earth Systems and Environment, 9*(1), 195-211. doi:10.1007/s40808-022-01492-6

Wang, H., Zhang, N., Niu, D., *et al.* (2024). Sources and formation of fine particles and organic aerosols during autumn-winter period in the southern edge of northern China plain. *Atmospheric Environment, 332*, 120614-. doi:10.1016/j.atmosenv.2024.120614

Wang, X., Bi, L., Wang, H., *et al.* (2025). AI-NAOS: an AI-based nonspherical aerosol optical scheme for the chemical weather model GRAPES_Meso5.1/CUACE. *Geosci. Model Dev., 18*(1), 117-139. doi:10.5194/gmd-18-117-2025

Wang, Y., Liu, F., He, C., *et al.* (2017). Fractal Dimensions and Mixing Structures of Soot Particles during Atmospheric Processing. *Environmental Science & Technology Letters, 4*(11), 487-493. doi:10.1021/acs.estlett.7b00418

Wang, Y., Pang, Y., Huang, J., *et al.* (2021). Constructing shapes and mixing structures of black carbon particles with applications to optical calculations. *Journal of Geophysical Research: Atmospheres, 126*(10), e2021JD034620.

Wang, Z., Bi, L., Wang, H., *et al.* (2022). Evaluation of a new internally-mixed aerosol optics scheme in the weather research and forecasting model. *Journal of Quantitative Spectroscopy and Radiative Transfer, 283*, 108147. doi:https://doi.org/10.5194/gmd-18-117-2025

Wenfei, Z., Song, G., Zirui, Z., *et al.* (2021). Mass spectral characterization of secondary organic aerosol from urban cooking and vehicular sources. *Atmospheric Chemistry and Physics, 21*(19), 15065-15079. doi:10.5194/acp-21-15065-2021

Wild, O., Zhu, X., & Prather, M. J. (2000). Fast-J: Accurate simulation of in-and below-cloud photolysis in tropospheric chemical models. *Journal of Atmospheric Chemistry, 37*, 245-282. doi:10.1023/A:1006415919030

Wriedt, T. (2012). Mie theory: a review. *The Mie theory: Basics and applications*, 53-71. doi:10.1007/978-3-642-28738-1

Xu, L., Zhang, D., & Li, W. (2019). Microscopic comparison of aerosol particles collected at an urban site in North China and a coastal site in Japan. *Science of the Total Environment, 669*, 948-954. doi:10.1016/j.scitotenv.2019.03.163

Zhang, R., Khalizov, A. F., Pagels, J., *et al.* (2008). Variability in morphology, hygroscopicity, and optical properties of soot aerosols during atmospheric processing. *Proceedings of the National Academy of Sciences of the United States of America, 105*(30), 6. doi:https://doi.org/10.1073/pnas.0804860105

https://doi.org/10.5194/egusphere-2026-4511
Preprint. Discussion started: 17 August 2026

900 Zhou, D., Ding, K., Huang, X., *et al.* (2018). Transport, mixing and feedback of dust, biomass burning and
901 anthropogenic pollutants in eastern Asia: a case study. *Atmospheric Chemistry and Physics, 18*(22), 16345-
902 16361. doi:10.5194/acp-2018-466
903
904